Vol. 88 No. 4 pp. 1169–1182 ACTA GEOLOGICA SINICA (English Edition) Aug. 2014

A New Method for Determining Fluid Compositions in the H_2O-NaCl-$CaCl_2$ System with Cryogenic Raman Spectroscopy

CHI Guoxiang[1,*], CHU Haixia[1], Ryan SCOTT[1] and CHOU I-Ming[2]

1 *Department of Geology, University of Regina, Regina, Saskatchewan, S4S 0A2, Canada*
2 *Laboratory for Experimental Study Under Deep-sea Extreme Conditions, Sanya Institute of Deep-sea Science and Engineering, Chinese Academy of Sciences, Sanya 572000, Hainan, China*

Abstract: Raman peaks of various hydrates in the H_2O-NaCl-$CaCl_2$ system have been previously identified, but a quantitative relationship between the Raman peaks and X_{NaCl} (i.e., NaCl/(NaCl+$CaCl_2$)) has not been established, mainly due to the difficulty to freeze the solutions. This problem was solved by adding alumina powder to the solutions to facilitate nucleation of crystals. Cryogenic (-185°C) Raman spectroscopic studies of alumina-spiced solutions indicate that X_{NaCl} is linearly correlated with the total peak area fraction of hydrohalite. Capsules of solutions made from silica capillary were prepared to simulate fluid inclusions. Most of these artificial fluid inclusions could not be totally frozen even at temperatures as low as -185°C, and the total peak area fraction of hydrohalite is not correlated linearly with X_{NaCl}. However, the degree of deviation (ΔX_{NaCl}) from the linear correlation established earlier is related to the amount of residual solution, which is reflected by the ratio (r) of the baseline "bump" area, resulting from the interstitial unfrozen brine near 3435 cm^{-1}, and the total hydrate peak area between 3350 and 3600 cm^{-1}. A linear correlation between ΔX_{NaCl} and r is established to estimate X_{NaCl} from cryogenic Raman spectroscopic analysis for fluid inclusions.

Key words: cryogenic, Raman, H_2O-NaCl-$CaCl_2$, X_{NaCl}, fluid inclusion

1 Introduction

Geologic fluids from a variety of environments, including sedimentary basins, metamorphic terrains, and various magmatic hydrothermal systems, can be approximated by the H_2O-NaCl-$CaCl_2$ system (Crawford, 1981; Vanko et al., 1988; Oakes et al., 1990; Williams-Jones and Samson, 1990; Chi et al., 1993, 1995, 1998, 2003b; Chi and Savard, 1995, 1997; Samson and Walker, 2000; Lavoie and Chi, 2005; Chi and Ni, 2007; Lai et al., 2007; Xue et al., 2007, 2010; Azmy et al., 2008; Wendte et al., 2009; Lavoie et al., 2010; Steele-MacInnis et al., 2011; Li et al., 2013). The composition of such fluids, characterized by the total salinity and NaCl/(NaCl+$CaCl_2$) molar ratio (X_{NaCl}), may be estimated from fluid inclusion studies using various analytical methods, including microthermometry (Haynes, 1985; Vanko et al., 1988; Oakes et al., 1990; Williams-Jones and Samson, 1990; Chi et al., 1993, 1995; Derome et al., 2005; Chi and Ni, 2007; Steele-MacInnis et al., 2011), decrepitation-SEM-EDS (Haynes and Kesler, 1987; Savard and Chi, 1998; Kontak, 2004), LA-ICP-MS or LIBS (Gunther et al., 1998; Fabre et al., 1999; Derome et al., 2005; Samson et al., 2008; Leisen et al., 2012), and various bulk-inclusions leachate analyses (Banks and Yardley, 1992; Gleeson et al., 2001). The microthermometry technique has the advantage of being single-inclusion analysis, non-destructive, and of high accessibility, but its use in determining X_{NaCl} is limited by the difficulty of accurately measuring the melting temperatures of various hydrates, although this problem may be partly solved by the cyclic freezing-heating technique (Haynes, 1985). The decrepitation-SEM-EDS and LA-ICP-MS or LIBS methods are also single-inclusion based, but they have the disadvantage of being destructive, as do the leachate analyses (see review by Chi et al., 2003a).

Raman spectroscopy has been well established as a single-inclusion, non-destructive, quantitative method of analysis of volatile composition of fluid inclusions (Pasteris et al., 1988; Dubessy et al., 1989; Frezzotti et al., 2012). It has also been widely used in identification of daughter minerals in fluid inclusions (Frezzotti et al.,

* Corresponding author. E-mail: guoxiang.chi@uregina.ca

2012), and can be used to estimate fluid pressure (Rosso and Bodnar, 1995; Lu et al., 2007; Song et al., 2009; Yang et al., 2009; Wang et al., 2011; Zheng et al., 2011). Semi-quantitative analysis has been possible for polyatomic ions and molecules in some cases (see Frezzotti et al., 2012 for a review), and methods of quantitative estimation of salinity based on the shape of O-H stretching band have been developed (Mernagh and Wilde, 1989; Dubessy et al., 2002; Sun et al., 2010; Wang et al., 2013). Dubessy et al. (2002) established quantitative relationships between chlorinity and Raman spectra of the stretching band of water for H_2O-NaCl-$CaCl_2$ solutions at different Na/Ca ratios, which may be potentially used to estimate Na/Ca ratios if the chlorinity can be accurately estimated using other methods. However, the analysis of monoatomic ions (Na^+, K^+, Ca^{2+}, and Mg^{2+}) with Raman spectroscopy has been generally of qualitative nature, mainly based on the recognition of Raman spectra of various NaCl and $CaCl_2$ salt-hydrates, including hydrohalite (NaCl•$2H_2O$), antarcticite ($CaCl_2$•$6H_2O$), α-tetrahydrate (α-$CaCl_2$•$4H_2O$), γ- tetrahydrate (γ-$CaCl_2$•$4H_2O$), and sinjarite ($CaCl_2$•$2H_2O$) (Table 1; Dubessy et al., 1982, 1992; Samson and Walker, 2000; Bakker, 2004; Derome et al., 2005; Baumgartner and Bakker, 2009a and b; 2010). The large number of peaks for these hydrates, the overlaps between some of them, the variation of measurements among different authors and at different temperatures (Table 1), and the dependence of peak intensity with crystal orientation (Baumgartner and Bakker, 2010), may appear to be major obstacles for quantitative studies. However, previous studies have shown that measurements within individual studies were fairly consistent, as discussed in Baumgartner and Bakker (2010), and only a few of the many bands of ice and hydrates are significant in the Raman spectra of the ice-hydrates aggregate (Samson and Walker, 2000). Furthermore, a visual correlation between the compositions of the H_2O-NaCl-$CaCl_2$ solutions and the intensities of the major peaks of hydrohalite and antarcticite can be perceived (Samson and Walker, 2000), suggesting that it is potentially possible to establish quantitative relationships between the intensities of the Raman bands of the hydrates and X_{NaCl}.

One of the main problems encountered in cryogenic Raman study of H_2O-NaCl-$CaCl_2$ solutions is the difficulty for the solution to be completely frozen, even at temperatures as low as -190°C (Samson and Walker, 2000; Baumgartner and Bakker, 2009a and b, 2010). Consequently, the proportions of NaCl and $CaCl_2$ hydrates in the solid aggregate of ice and hydrates may not reflect the initial X_{NaCl} value of the solution, which makes it impossible to determine the composition of the solution through Raman spectroscopic measurement of the hydrates. In this paper, we developed a new method to completely freeze the solution by adding alumina powder into the solution, and established a linear relationship between the Raman spectra of the hydrates and X_{NaCl}. We further demonstrated that for fluid inclusions that cannot be completely frozen, simulated with solutions capsulated

Table 1 Raman peaks of ice and hydrates in the H_2O-NaCl-$CaCl_2$ system

Solid phase	Raman peaks (cm^{-1})	Condition of measurement	References
Ice (H_2O)	3090 (main), 3250 (minor)	−190°C	Dubessy et al., 1982
	3092 (main), 3216 (minor)	−175 to −185°C	Samson and Walker, 2000
	3105 (main), 3228 (minor)	−170°C	Bakker, 2004
	3098 (main)	−180°C	Ni et al., 2006
	3096±3 (main), 3218 and 3321 (broad band)	−190°C	
	3073 (main)	−190°C; initial freezing of an "all-liquid" fluid inclusion	Baumgartner and Bakker, 2010
	3096 (main)	Re-cooled to −190°C after recrystallization	
Hydrohalite (NaCl•$2H_2O$)	3406, 3422, 3438, 3536	−170°C	Dubessy et al., 1982
	3403, 3420, 3435, 3536	−175 to −185°C	Samson and Walker, 2000
	3326, 3407, 3424, 3439, 3539	−190°C	Bakker, 2004
	3405, 3423, 3437, 3538	−180°C	Ni et al., 2006
	3402±2, 3418±1, 3432±2, 3536±4	−190°C	Baumgartner and Bakker, 2010
Antarcticite ($CaCl_2$•$6H_2O$)	3383, 3402, 3407, 3427, 3448 and 3513 (minor)	−170°C	Dubessy et al., 1982
	3386, 3406, 3432	−175 to −185°C	Samson and Walker, 2000
	3240±2, 3387±2, 3402±2, 3430±1	−190°C	Baumgartner and Bakker, 2009b
	3386±2, 3405±2, 3410±2, 3430±1, 3242±3 (minor)	−190°C	Baumgartner and Bakker, 2010
α-tetrahydrate (α-$CaCl_2$•$4H_2O$)	3197±2, 3369±6, 3425±3, 3446±2	−190°C	Baumgartner and Bakker, 2009b
	3365±6 and 3445±2 (main); 3423±3 and 3475±5 (shoulders); 3365, 3196, and 3216 (broad)	−190°C	Baumgartner and Bakker, 2010
γ-tetrahydrate (γ-$CaCl_2$•$4H_2O$)	3435	−190°C	Baumgartner and Bakker, 2009b
	3434 (main); 3260, 3392, 3463 and 3575 (shoulders)	−190°C	Baumgartner and Bakker, 2010
Sinjarite ($CaCl_2$•$2H_2O$)	3377±1, 3405±3, 3424±2, 3464±2; 3559±2	−190°C	Baumgartner and Bakker, 2009b
	3424±2 and 3376±1 (main); 3403±3 (minor); 3462 – 3471 (broad); 3190±2, 3242±9, 3285±4, 3318±5, 3352±4 and 3557±2 (shoulders)	−190°C	Baumgartner and Bakker, 2010

in fused silica capillary, a quantitative relationship between the Raman spectra of the hydrates and X_{NaCl} can still be established depending on the degree of freezing, as reflected by the relative amplitude of the baseline due to the water band caused by the residual interstitial solution. The analytical errors and potential problems in application to fluid inclusion studies are discussed based on the experimental results.

2 Experimental and Analytical Methods

A total of 11 solutions, with a salinity of 15 mass% NaCl+$CaCl_2$ and different NaCl molar ratios (X_{NaCl}), were prepared from sodium chloride (EMD Chemicals Inc., lot TG29AZEMS) and calcium chloride (VWR International, lot ZH2631NFAE) and deionized water. The solutions were labeled from #1 to #11 with X_{NaCl} decreased continuously from 1.0 to 0.0 at an increment of -0.1. Two sets of experiments were carried out with these solutions: (1) the sandwiched experiments, in which the solution was mixed with alumina powder and sandwiched between two thin glass slides; and (2) the capillary experiments, in which the solution was sealed in silica capillary tubes. The first set of experiments attempts to use alumina particles to facilitate nucleation of ice and hydrate crystals, in order to achieve complete freezing of the solution, whereas the second set aims to simulate natural fluid inclusions.

In the sandwiched experiments, alumina powder (0.05 microns) was added to the solution in a plastic bottle, which was thoroughly shaken before sampling. A droplet of the alumina-solution mixture was placed between two small pieces (about 5-10 mm wide) of thin glass, which was then placed in a Linkam TMHS600 heating-freezing stage for cryogenic Raman analysis. In the capillary experiments, the solution was loaded into a silica capillary tube with an inner diameter of 50 microns, an outer diameter of 300 microns and a length of about 1 cm, and the tube was then sealed by fusion using the method of Chou et al. (2008). The fused capillary tubes were also analyzed with cryogenic Raman spectroscopy. Various combinations of temperatures and cooling rates were used for both sets of experiments to achieve maximum freezing.

Raman analysis was carried out with a Renishaw RM2000 laser Raman spectroscope at the Geofluids Laboratory of the University of Regina. The excitation laser wavelength is 514 nm, the grating used is 1800, and the objective is ×50 with long working distance. All the analyses were done at a temperature of -185°C. Data were collected between 3000 and 3800 cm^{-1}, which covered the essential peaks of ice and hydrates in the H_2O-NaCl-$CaCl_2$ system (Samson and Walker, 2000; Baumgartner and Bakker, 2010) (Table 1). The procedure of data acquisition and methods of data treatment, together with the results of experiments, are described for the sandwiched experiments and capillary experiments separately as follows.

3 Sandwiched Experiments

Microscopic observations at room temperature indicate that particles of alumina, a few microns in size, were dispersed in the solution. The samples were cooled from room temperature to -60°C at a cooling rate of 30°C/minute, and then to -185°C at a cooling rate of 2°C/minute. All the samples showed a sudden freezing event at a temperature between -30 and -40°C, when ice was crystallized to form a solid framework with remaining solution in interstitial space. The high cooling rate facilitated the formation of a homogeneous ice-solution mixture, which is necessary for the composition (either fluid + solids, in the case of incomplete freezing, or entirely solids, in the case of complete freezing) to be uniform across the sample. Further cooling led to crystallization of various hydrates, accompanied by darkening of the sample. The degree of freezing is uneven in a given sample, reflected by areas of different darkness (Fig. 1). Raman analysis indicated that the darkest part of a sample, generally occurring as patches of variable sizes, was totally frozen, whereas the lighter parts contain variable amount of unfrozen solution.

For each sample, 6 data points (in the darkest areas) were analyzed with Raman spectroscopy at -185°C, with each data point consisting of 10 consecutive acquisitions of 10 seconds each. The laser spot was manually moved a few microns from one acquisition to another in order to reduce the potential effect of inhomogeneity due to the presence of coarse crystals and locally preferred orientation of crystals. After the Raman analysis, the sample was gradually heated to obtain the melting temperatures of hydrohalite and ice (heating rate was 0.1°C near the melting points). The microthermometric results indicate that the ice-melting temperatures are variably deviated from the theoretically expected values, suggesting variable water loss (due to evaporation) during the sample preparation and experimental procedures, but the hydrohalite-melting temperatures are within 0.5°C of the values predicted from previous studies of the H_2O-NaCl-$CaCl_2$ system (Chi and Ni, 2007), suggesting that the X_{NaCl} values were not affected by the sample preparation and experimental procedures.

The representative Raman spectra of each sample are shown in Fig. 2. A prominent peak at 3422 cm^{-1} (peak 3) and one at 3537 cm^{-1} (peak 6) are attributed to hydrohalite, two peaks at 3405-3408 cm^{-1} (peak 2) and 3434-3437 cm^{-1}

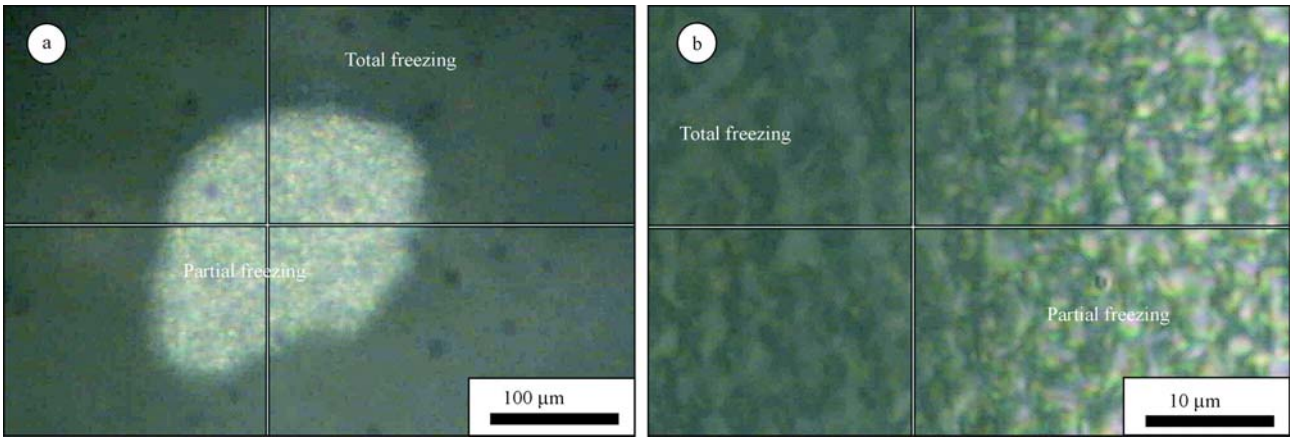

Fig. 1. Photomicrographs showing different degrees of freezing of the solution (sandwiched between thin glass slides) at -185°C, as reflected by the variation of darkness of the sample.
The darkest part is totally frozen (i.e., no remaining solution among ice and hydrate crystals), whereas the light parts consist mainly of ice and interstitial solution. (a), A light-colored pocket of ice and solution within a dark mixture of ice and hydrates; (b), transition from a totally frozen part (dark) to a partly frozen part (relatively light).

(peak 4) are due to combined hydrohalite and antarcticite contributions, and two "shoulders", one to the left of the combined 3405-3408 cm^{-1} peak (peak 1) and the other to the right of the combined 3434-3437 cm^{-1} peak (peak 5), are due to combined contributions of antarcticite, α-$CaCl_2$•$4H_2O$ and sinjarite. The area fraction of individual peaks is calculated as $a_i = A_i/\Sigma A_i$, where i = 1 to 6. The total area fraction of bands attributed to NaCl hydrate or hydrohalite is $a_{Na} = a_3+a_6$, and the total area fraction of bands attributed to $CaCl_2$ hydrates is $a_{Ca} = a_1+a_5$, whereas the total area fraction of bands attributed to undivided hydrohalite and $CaCl_2$ hydrates is $a_{NaCa} = a_2+a_4$. In some cases, a peak at 3416 cm^{-1} attributed to α-$CaCl_2$•$4H_2O$ is distinguishable and the area is added to a_{Ca}. The area fraction of individual bands ($a_1 - a_6$) and other parameters including a_{Na}, a_{Ca}, and a_{NaCa} of all the experimental runs are listed in Table 2.

A clear positive correlation is shown between a_{Na} and X_{NaCl} (Fig. 3a). However, the correlation is non-linear, which can be explained by the fact that the contribution of hydrohalite is not only reflected in peaks 3 and 6 (a_{Na}), but also partly in peaks 2 and 4 (a_{NaCa}); the total contribution of hydrohalite should be equal to $a_{Na}+X_{NaCl}*a_{NaCa}$. Plotting $a_{Na}+X_{NaCl}*a_{NaCa}$ against X_{NaCl} shows a well-defined linear correlation (Fig. 3b). This linear correlation, with the interception close to zero and the slope close to 1, confirms the theoretical expectation that the fraction of NaCl molecules in the solution (i.e., X_{NaCl}) is equal to the fraction of NaCl•$2H_2O$ molecules in the aggregates of salt hydrates (if the solution is completely frozen), which can be expressed as:

$$a_{Na}+X_{NaCl}*a_{NaCa} = X_{NaCl} \quad (1)$$

Rearranging equation (1), we get:

$$X_{NaCl} = a_{Na}/(1-a_{NaCa}) \quad (2)$$

which defines X_{NaCl} as a function of a_{Na} and a_{NaCa}.

4 Capillary Experiments

The capillary experiments were designed to simulate fluid inclusions in order to see if the linear correlation established in the sandwiched experiments can be applied to fluid inclusion analysis. When the capillary samples were cooled rapidly (30°C/minute) from room temperature (Fig. 4a) to -185°C, most of them show sudden freezing at a temperature between -60 and -100°C (Fig. 4b), but some did not freeze, and showed slight stretching of the air bubble (Fig. 4c), with a broad water band peaked at 3430 cm^{-1} (Fig. 4d). For those that seem to have totally frozen during the first cooling to -185°C, as suggested by the dark color (Fig. 4e), Raman signals showed only ice (3009 and 3225 cm^{-1}) and water (3416 cm^{-1}) bands, without those for hydrates (Fig. 4f), suggesting incomplete freezing. These samples were then slowly (2°C/minute) warmed to -60°C and then rapidly cooled to -185°C again (Fig. 4g), which in many cases resulted in significant growth of hydrates, as indicated by hydrate peaks in the Raman spectra (Fig. 4h). However, even in these runs, some residual solution may still remain in interstitial space, as suggested by the raised baseline around the water peak (compare the spectra of Figs. 4f and h), hereinafter called the "water bump". The solution was frozen to different extents within a given sample, and Raman spectroscopic data were collected from areas that showed relatively high degree of freezing, with an acquisition time of 60 seconds at a fixed spot.

The representative spectra of each sample in the capillary experiments are shown in Fig. 5. The Raman spectra were treated as follows: 1) truncate the spectra between 3350 to 3600 cm^{-1} (which covers the most

important peaks of hydrates of NaCl and $CaCl_2$), make a straight baseline connecting the two ends of the spectra, conduct baseline subtraction (Fig. 6a) and calculate the total area of the spectra (TA1); 2) use the "Cubic Spline Interpretation" function and anchor points at 3370, 3435, 3500 and 3570 cm^{-1} to make a new baseline to approximate the "water bump" (Fig. 6b); 3) make baseline subtraction (Fig. 6c) and calculate the total area of the spectra (TA2); 4) calculate the area contributed by the "water bump": w = TA1-TA2; and 5) calculate the area of individual Raman bands (A_i) with the Lorentzian curve-fitting function: when peaks are well defined in the original spectra (e.g., peaks 2, 3, 4 and 6 in Fig. 6c), peak center, width and height are allowed to float, but when there is no visible peak in the original spectra (e.g., "peaks" 1 and 5 in Fig. 6c), a fixed peak center (e.g., 3385 cm^{-1} for antarcticite and 3471 cm^{-1} for combined α - $CaCl_2.4H_2O$ and sinjarite) is assigned. It is important to follow the same procedure for all runs for consistency of calculation results.

The area fraction of individual bands (a_1 – a_6), the "water bump" to total peak area ratio (r) and other parameters, including a_{Na} and a_{NaCa}, are listed in Table 3. The correlation

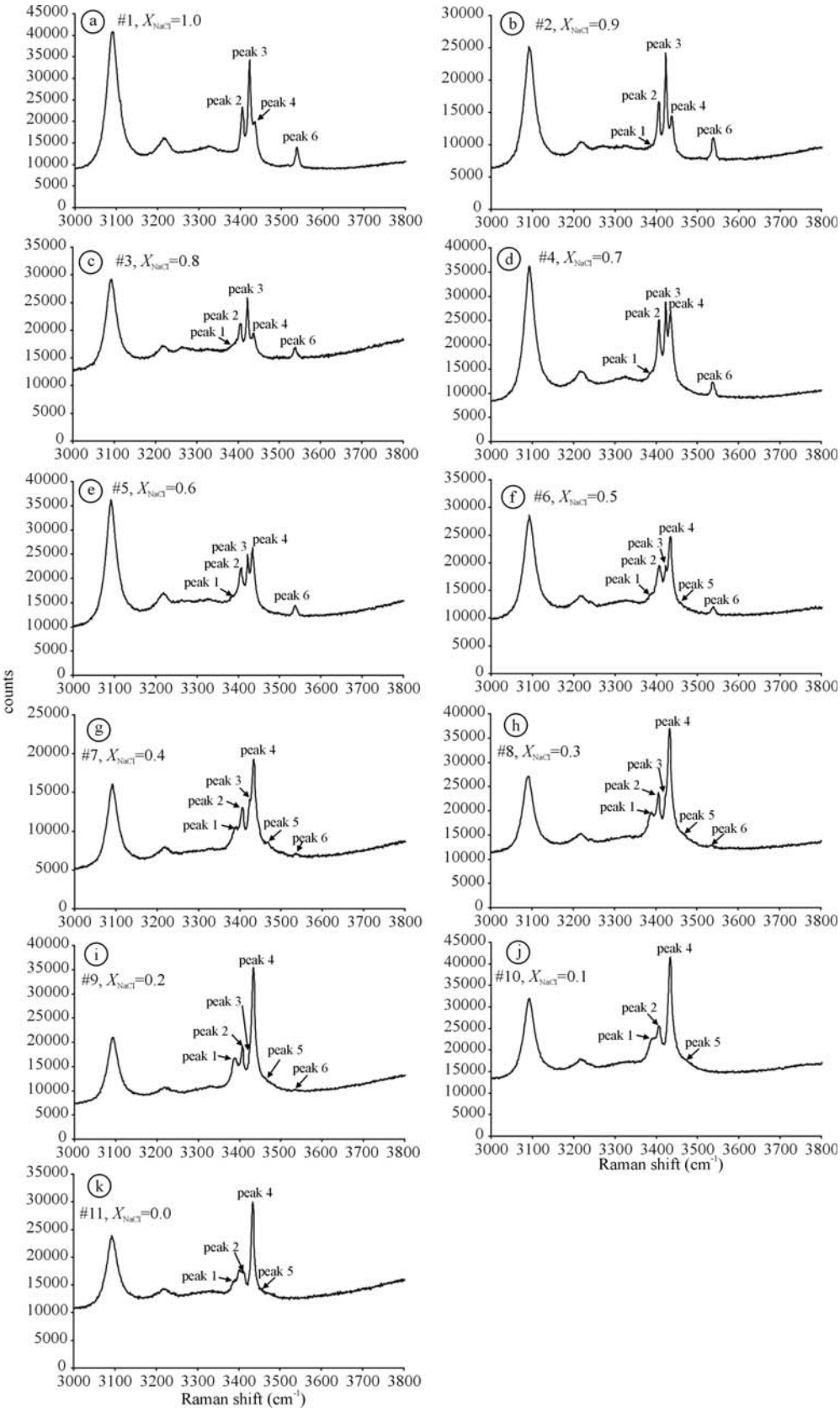

Fig. 2. Representative Raman spectra of H_2O-NaCl-$CaCl_2$ solutions with different X_{NaCl} values in the sandwiched experiments. The solutions have been mixed with alumina powder to facilitate complete freezing.

Table 2 Raman spectroscopic results of sandwiched experiments

Sample #	Runs	Spot	X_{NaCl}	a_1	a_2	a_3	a_4	a_5	a_6	a_{Na}	a_{NaCa}	$a_{Na}+X_{NaCl}*a_{NaCa}$
1	1	1	1.000	0.000	0.238	0.440	0.227	0.000	0.096	0.536	0.464	1.000
		2	1.000	0.000	0.213	0.446	0.212	0.000	0.129	0.575	0.425	1.000
		3	1.000	0.000	0.178	0.368	0.242	0.000	0.213	0.580	0.420	1.000
		4	1.000	0.000	0.228	0.434	0.222	0.000	0.116	0.550	0.450	1.000
		5	1.000	0.000	0.157	0.339	0.241	0.000	0.264	0.602	0.398	1.000
		6	1.000	0.000	0.185	0.417	0.227	0.000	0.170	0.587	0.413	1.000
2	1	1	0.900	0.021	0.232	0.412	0.228	0.000	0.106	0.518	0.460	0.933
		2	0.900	0.027	0.224	0.392	0.232	0.000	0.124	0.516	0.457	0.927
		3	0.900	0.048	0.224	0.338	0.315	0.002	0.073	0.411	0.540	0.896
		4	0.900	0.033	0.268	0.348	0.294	0.010	0.047	0.395	0.562	0.901
		5	0.900	0.033	0.180	0.347	0.307	0.000	0.133	0.480	0.488	0.918
		6	0.900	0.040	0.179	0.280	0.330	0.028	0.142	0.423	0.509	0.881
3	1	1	0.800	0.053	0.219	0.369	0.245	0.000	0.114	0.483	0.464	0.854
		2	0.800	0.081	0.257	0.342	0.218	0.000	0.102	0.444	0.475	0.824
		3	0.800	0.099	0.246	0.348	0.214	0.000	0.093	0.441	0.460	0.809
		4	0.800	0.037	0.252	0.359	0.252	0.000	0.100	0.459	0.504	0.862
		5	0.800	0.114	0.201	0.292	0.298	0.000	0.096	0.388	0.499	0.787
		6	0.800	0.022	0.234	0.251	0.415	0.000	0.077	0.329	0.649	0.848
4	1	1	0.700	0.047	0.267	0.179	0.418	0.033	0.055	0.235	0.685	0.714
		2	0.700	0.016	0.259	0.229	0.384	0.005	0.107	0.336	0.643	0.786
		3	0.700	0.020	0.261	0.246	0.352	0.000	0.120	0.367	0.613	0.796
		4	0.700	0.046	0.248	0.183	0.421	0.027	0.076	0.258	0.669	0.726
		5	0.700	0.059	0.257	0.176	0.388	0.061	0.058	0.234	0.645	0.686
		6	0.700	0.020	0.263	0.218	0.392	0.009	0.097	0.315	0.656	0.774
5	1	1	0.600	0.037	0.287	0.080	0.496	0.043	0.057	0.138	0.783	0.607
		2	0.600	0.040	0.300	0.145	0.450	0.000	0.066	0.210	0.750	0.660
		3	0.600	0.052	0.297	0.116	0.472	0.000	0.063	0.179	0.769	0.640
		4	0.600	0.055	0.277	0.106	0.456	0.063	0.043	0.149	0.733	0.588
		5	0.600	0.075	0.298	0.170	0.352	0.044	0.061	0.231	0.650	0.620
		6	0.600	0.019	0.319	0.214	0.377	0.038	0.033	0.247	0.696	0.665
6	1	1	0.500	0.041	0.330	0.142	0.423	0.016	0.047	0.189	0.753	0.566
		2	0.500	0.051	0.325	0.125	0.411	0.042	0.045	0.170	0.737	0.538
		3	0.500	0.049	0.305	0.037	0.506	0.075	0.028	0.065	0.811	0.471
		4	0.500	0.035	0.298	0.048	0.511	0.068	0.040	0.088	0.809	0.492
		5	0.500	0.042	0.312	0.075	0.473	0.055	0.044	0.119	0.785	0.511
		6	0.500	0.027	0.350	0.057	0.460	0.059	0.047	0.104	0.810	0.509
7	2	1	0.400	0.066	0.426	0.121	0.354	0.000	0.032	0.153	0.780	0.466
		2	0.400	0.088	0.231	0.015	0.519	0.148	0.000	0.015	0.749	0.314
		3	0.400	0.142	0.192	0.020	0.525	0.121	0.000	0.020	0.717	0.307
		4	0.400	0.120	0.189	0.048	0.565	0.070	0.008	0.055	0.755	0.357
		5	0.400	0.076	0.271	0.053	0.495	0.081	0.024	0.077	0.767	0.383
		6	0.400	0.101	0.245	0.008	0.514	0.132	0.000	0.008	0.759	0.311
8	1	7	0.300	0.177	0.185	0.012	0.515	0.101	0.009	0.021	0.701	0.231
		8	0.300	0.143	0.216	0.014	0.556	0.071	0.000	0.014	0.772	0.246
		9	0.300	0.152	0.134	0.016	0.549	0.146	0.003	0.019	0.683	0.224
		10	0.300	0.159	0.134	0.018	0.564	0.119	0.006	0.024	0.698	0.233
		11	0.300	0.151	0.144	0.020	0.577	0.101	0.008	0.027	0.721	0.244
		12	0.300	0.150	0.135	0.017	0.585	0.107	0.006	0.024	0.720	0.240
9	1	1	0.200	0.167	0.159	0.000	0.561	0.113	0.000	0.000	0.720	0.144
		2	0.200	0.174	0.119	0.004	0.575	0.127	0.001	0.005	0.694	0.144
		3	0.200	0.184	0.091	0.001	0.600	0.122	0.001	0.002	0.692	0.140
		4	0.200	0.170	0.097	0.001	0.584	0.143	0.004	0.006	0.681	0.142
		5	0.200	0.182	0.109	0.000	0.587	0.115	0.006	0.006	0.696	0.145
		6	0.200	0.211	0.108	0.000	0.550	0.131	0.000	0.000	0.658	0.132
10	1	1	0.100	0.096	0.263	0.000	0.492	0.149	0.000	0.000	0.756	0.076
		2	0.100	0.176	0.146	0.000	0.548	0.130	0.000	0.000	0.694	0.069
		3	0.100	0.178	0.126	0.000	0.563	0.133	0.000	0.000	0.689	0.069
		4	0.100	0.195	0.124	0.000	0.555	0.125	0.000	0.000	0.679	0.068
		5	0.100	0.173	0.147	0.000	0.573	0.108	0.000	0.000	0.720	0.072
		6	0.100	0.186	0.125	0.000	0.556	0.132	0.000	0.000	0.681	0.068
11	1	2	0.000	0.106	0.324	0.000	0.455	0.115	0.000	0.000	0.780	0.000
		3	0.000	0.166	0.168	0.000	0.551	0.115	0.000	0.000	0.719	0.000
		4	0.000	0.205	0.173	0.000	0.553	0.069	0.000	0.000	0.727	0.000
		5	0.000	0.169	0.213	0.000	0.563	0.056	0.000	0.000	0.775	0.000
		6	0.000	0.140	0.209	0.000	0.518	0.133	0.000	0.000	0.727	0.000

* See text for meaning of the parameters.

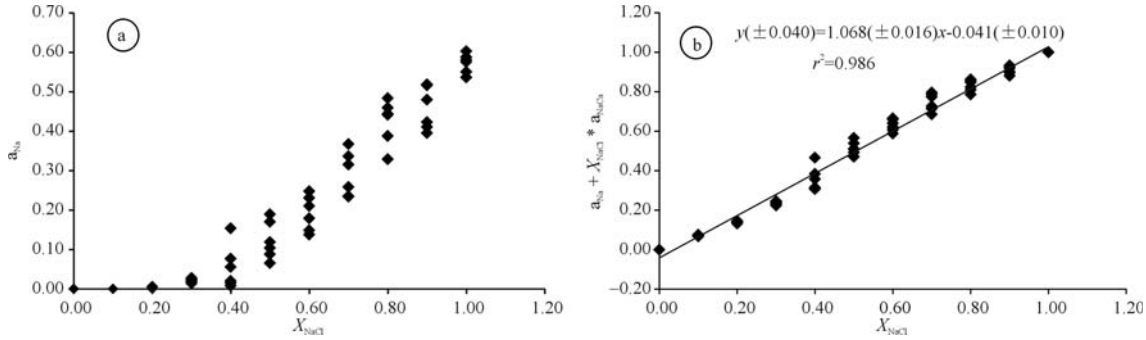

Fig. 3. a) Correlation between X_{NaCl} and area fraction of hydrohalite peaks (a_{Na}); b) Correlation between X_{NaCl} and fraction of hydrohalite peaks plus the contribution of hydrohalite in combined hydrohalite and antarcticite peaks.

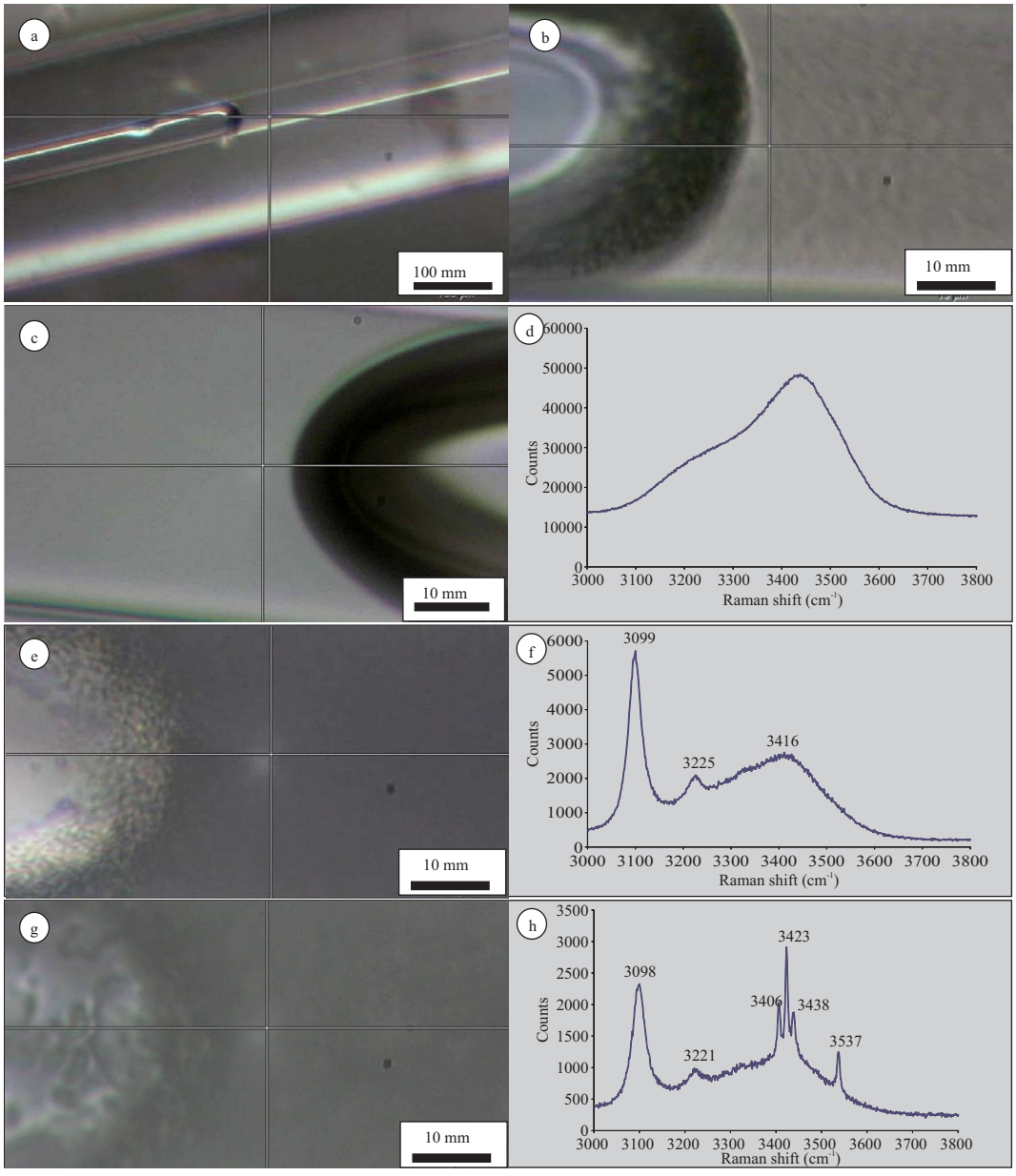

Fig. 4. Photomicrographs and Raman spectra of the capillary experiments.
(a), A silica capillary filled with solution and an air bubble at room temperature; (b), a capillary solution sample showing initial freezing (ice crystallization) at −69°C; (c), a capillary solution sample that did not freeze at −185°C (note the air bubble is slightly stretched); (d), Raman spectra of c showing a broad water band; (e), a capillary solution sample that appeared totally frozen when it was cooled to −185°C for the first time; (f), Raman spectra of e suggesting the lack of hydrates or incomplete freezing; (g), the same sample as f, this time slowly warmed to −60°C and then rapidly cooled to −185°C again, (h), Raman spectra of g indicating crystallization of abundant hydrates.

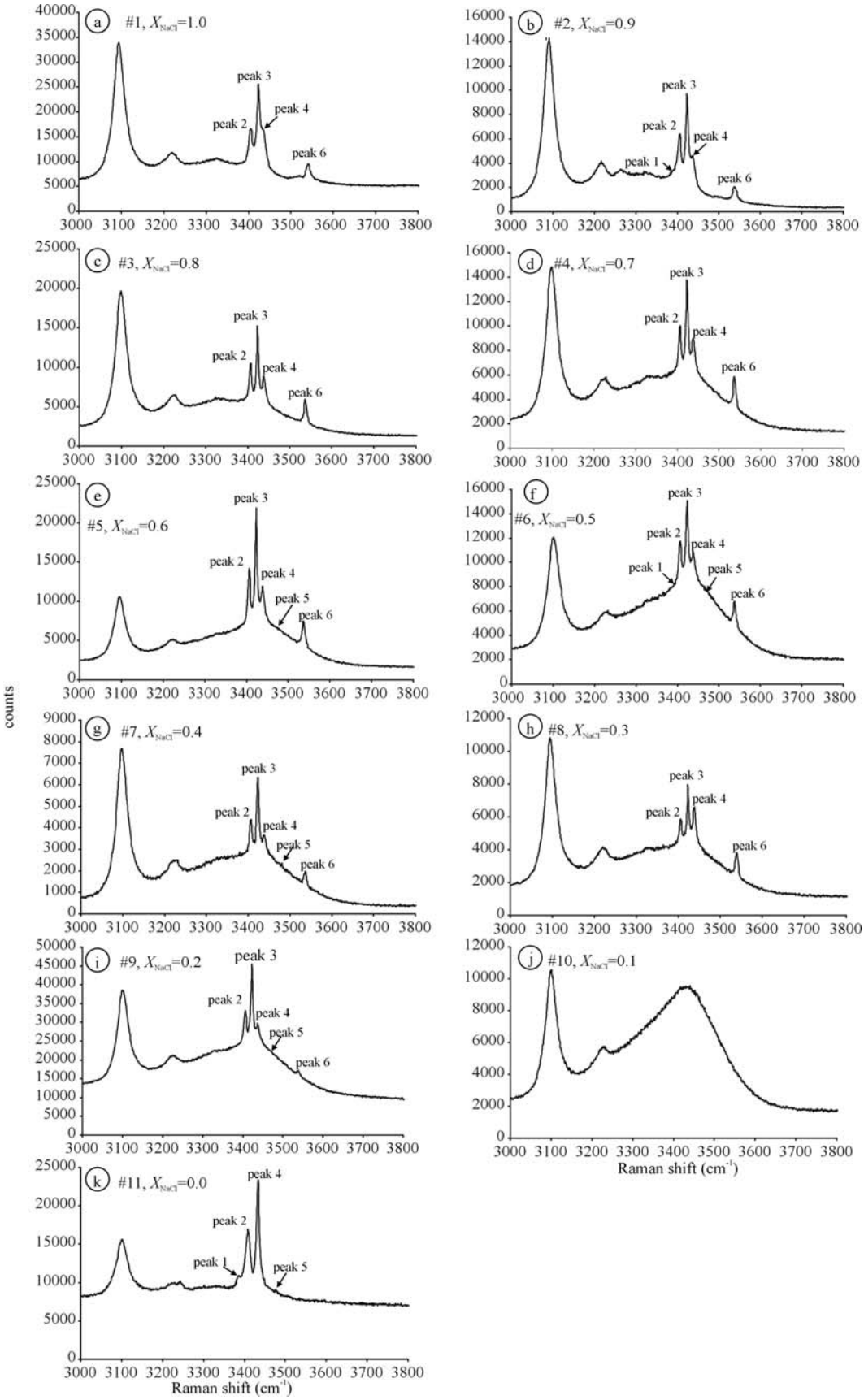

Fig. 5. Representative Raman spectra of H_2O-NaCl-$CaCl_2$ solutions with different X_{NaCl} values in the capillary experiments. The solutions do not contain alumina powder and the freezing is incomplete.

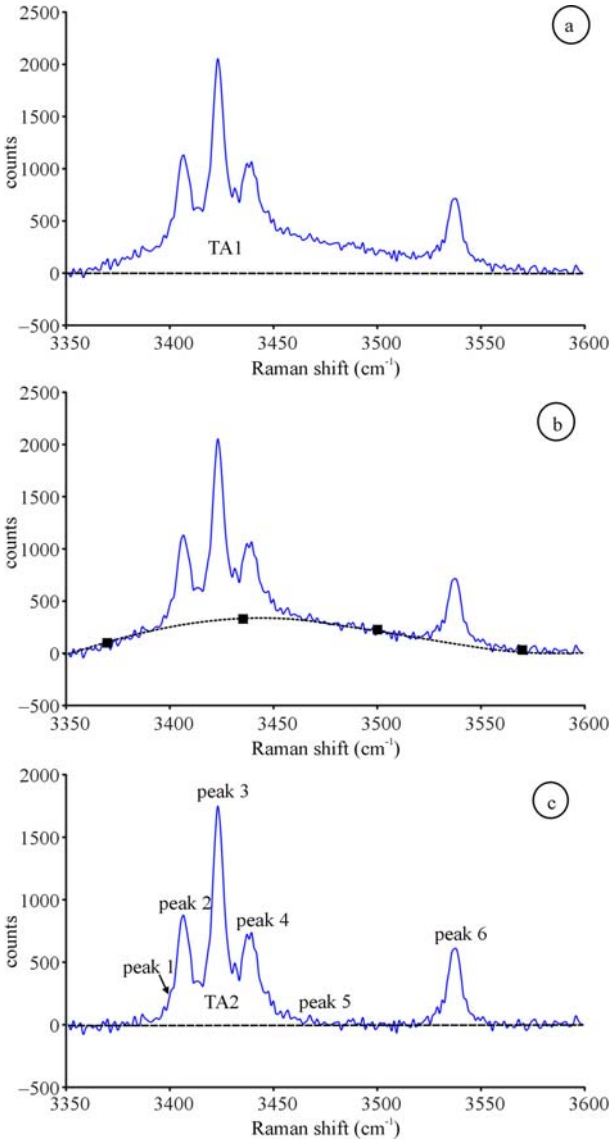

Fig. 6. Raman spectra of NaCl-$CaCl_2$-H_2O fluid synthesized in fused silica capillary capsules and baseline subtraction procedures.
(a), Raman spectra truncated between 3350 and 3600 cm^{-1} followed by a straight baseline (linking the two end points) subtraction; TA1 represents the total area of the spectra after baseline subtraction; (b), construction of a new baseline using the "Cubic Spline Interpretation" function to approximate the "water bump", with anchor points at 3370, 3435, 3500 and 3570 cm^{-1}; (c), Raman spectra after subtraction of the baseline shown in b (TA2 represents the total area after baseline subtraction). The meaning of pk1-6 is explained in the text.

between X_{NaCl} and $a_{Na}/(1-a_{NaCa})$ is shown in Fig. 7, which is far from the one-to-one linear relationship predicted from equation (2). The difference between the measured $a_{Na}/(1-a_{NaCa})$ value and the expected one (which is equal to X_{NaCl} according to equation 2) is expressed as:

$$\Delta X_{NaCl} = a_{Na}/(1-a_{NaCa}) - X_{NaCl} \quad (3)$$

It was found that ΔX_{NaCl} is somewhat related to the "water bump" to total peak area ratio (r), as shown in Fig. 8a. An inspection of this diagram indicates that there is a linear correlation between ΔX_{NaCl} and r if r is ≤ 1 (Fig. 8b),

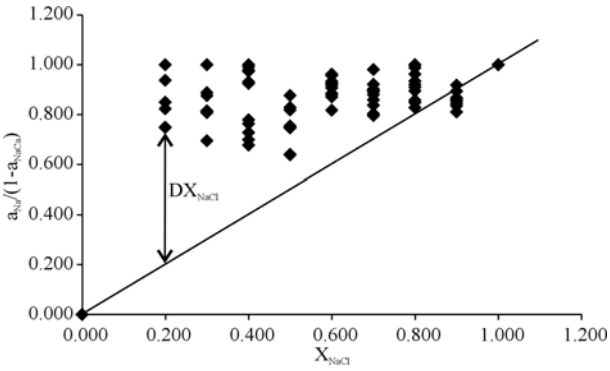

Fig. 7. Correlation between X_{NaCl} and $a_{Na}/(1-a_{NaCa})$ of the capillary experiments. The line represents the expected relationship for complete freezing. The difference between the measured and expected values is indicated by X_{NaCl}.

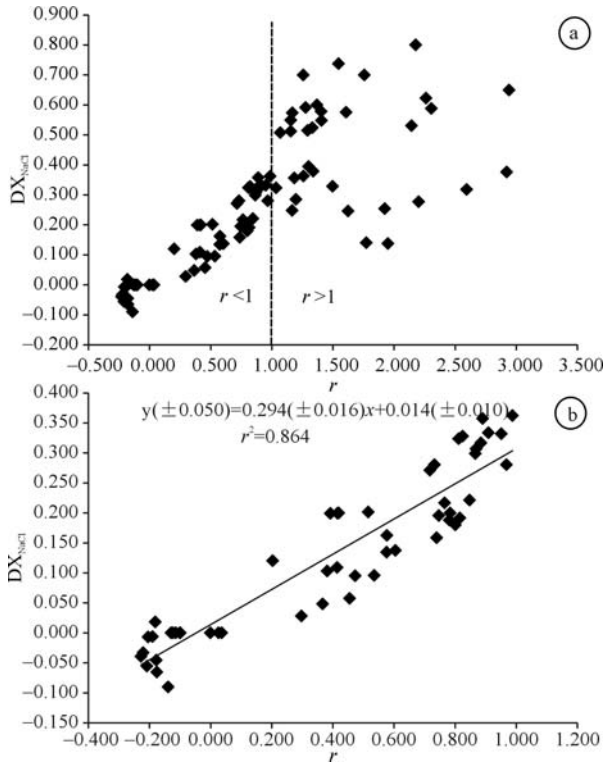

Fig. 8. Relationship between ΔX_{NaCl} and the ratio of "water bump" to total peak areas (r) for all capillary experiments (a) and for r<1 (b).

which can be expressed as:

$$\Delta X_{NaCl} = 0.294\, r + 0.014 \quad (4)$$

It is noticed that solutions that satisfy this condition are mainly those with $X_{NaCl} \geq 0.4$. Although the statistical analysis of the data indicates considerable errors for equation (4) (e.g., ±0.050 for the estimated ΔX_{NaCl}, Fig. 8b), the equation provides an opportunity to quantitatively estimate X_{NaCl} from the Raman peaks when the water bump is not too high (i.e., $r \leq 1$). Combining equations (3) and (4), the "corrected" correlation between X_{NaCl} and the total peak area fraction contributed by hydrohalite can be expressed as:

Table 3 Raman spectroscopic results of capillary experiments

Sample #	Runs	Spot	X_{NaCl}	a_1	a_2	a_3	a_4	a_5	a_6	r	a_{Na}	a_{NaCa}	$a_{Na}/(1-a_{NaCa})$	X_{NaCl}	Calculated X_{NaCl}
1-1	2	1	1.000	0.000	0.213	0.433	0.247	0.000	0.106	−0.099	0.540	0.460	1.000	0.000	1.016
		2	1.000	0.000	0.208	0.418	0.251	0.000	0.123	−0.123	0.541	0.459	1.000	0.000	1.023
		3	1.000	0.000	0.203	0.411	0.255	0.000	0.131	−0.100	0.542	0.458	1.000	0.000	1.016
		4	1.000	0.000	0.194	0.416	0.261	0.000	0.129	−0.129	0.545	0.455	1.000	0.000	1.024
		5	1.000	0.000	0.192	0.416	0.261	0.000	0.131	−0.114	0.547	0.453	1.000	0.000	1.020
2	2	1	0.900	0.106	0.246	0.360	0.195	0.000	0.092	−0.138	0.453	0.441	0.810	−0.090	0.837
		2	0.900	0.072	0.240	0.371	0.219	0.000	0.097	−0.220	0.469	0.460	0.867	−0.033	0.918
		3	0.900	0.089	0.187	0.371	0.242	0.000	0.111	−0.208	0.482	0.429	0.845	−0.055	0.892
		4	0.900	0.057	0.238	0.359	0.231	0.000	0.115	−0.204	0.474	0.469	0.893	−0.007	0.940
		5	0.900	0.044	0.243	0.376	0.219	0.000	0.118	−0.180	0.494	0.462	0.918	0.018	0.958
		6	0.900	0.082	0.218	0.413	0.215	0.000	0.071	−0.177	0.484	0.433	0.855	−0.045	0.893
		7	0.900	0.090	0.234	0.341	0.220	0.000	0.115	−0.175	0.455	0.455	0.835	−0.065	0.873
		9	0.900	0.076	0.229	0.320	0.226	0.000	0.149	−0.227	0.469	0.456	0.861	−0.039	0.914
		10	0.900	0.059	0.223	0.378	0.220	0.000	0.121	−0.190	0.498	0.443	0.894	−0.006	0.936
3	1	1	0.800	0.000	0.220	0.412	0.214	0.000	0.153	0.416	0.566	0.434	0.999	0.199	0.866
		2	0.800	0.000	0.218	0.408	0.220	0.000	0.154	0.420	0.563	0.437	1.000	0.200	0.866
		3	0.800	0.055	0.193	0.372	0.204	0.031	0.145	0.456	0.517	0.397	0.858	0.058	0.713
	2	1	0.800	0.054	0.206	0.371	0.201	0.036	0.133	0.367	0.504	0.406	0.848	0.048	0.729
		2	0.800	0.005	0.208	0.418	0.196	0.002	0.170	0.782	0.589	0.404	0.988	0.188	0.749
		3	0.800	0.015	0.204	0.371	0.222	0.045	0.143	0.473	0.514	0.425	0.895	0.095	0.745
		4	0.800	0.039	0.213	0.377	0.216	0.007	0.148	0.203	0.525	0.429	0.920	0.120	0.849
		5	0.800	0.028	0.199	0.370	0.218	0.025	0.160	0.414	0.530	0.417	0.909	0.109	0.776
		6	0.800	0.004	0.205	0.389	0.208	0.018	0.177	0.577	0.565	0.413	0.963	0.163	0.783
		7	0.800	0.000	0.215	0.406	0.206	0.000	0.174	0.393	0.580	0.420	0.999	0.199	0.873
		8	0.800	0.000	0.214	0.432	0.180	0.000	0.174	0.784	0.606	0.394	1.000	0.200	0.760
		9	0.800	0.004	0.209	0.404	0.194	0.035	0.155	0.577	0.559	0.402	0.935	0.135	0.755
		10	0.800	0.046	0.197	0.359	0.200	0.058	0.140	0.298	0.499	0.397	0.828	0.028	0.729
4	2	1	0.700	0.000	0.228	0.413	0.222	0.011	0.126	0.733	0.539	0.450	0.980	0.280	0.755
		2	0.700	0.004	0.190	0.376	0.223	0.059	0.147	0.816	0.523	0.413	0.892	0.192	0.643
		3	0.700	0.026	0.199	0.342	0.272	0.037	0.124	0.801	0.465	0.471	0.880	0.180	0.635
		4	0.700	0.034	0.193	0.355	0.215	0.062	0.141	0.605	0.496	0.408	0.837	0.137	0.649
		5	0.700	0.050	0.188	0.340	0.221	0.066	0.135	0.382	0.475	0.409	0.803	0.103	0.680
		6	0.700	0.014	0.202	0.393	0.209	0.047	0.135	0.748	0.527	0.411	0.895	0.195	0.666
		7	0.700	0.000	0.178	0.348	0.249	0.045	0.180	0.848	0.527	0.428	0.921	0.221	0.663
		8	0.700	0.017	0.199	0.379	0.213	0.041	0.150	0.517	0.530	0.412	0.902	0.202	0.739
		9	0.700	0.074	0.194	0.345	0.217	0.046	0.124	0.536	0.469	0.411	0.796	0.096	0.628
		10	0.700	0.039	0.201	0.382	0.195	0.047	0.137	0.740	0.518	0.397	0.859	0.159	0.632
5	1	1	0.600	0.000	0.186	0.356	0.219	0.069	0.171	1.198	0.527	0.404	0.885	0.285	0.525
		2	0.600	0.006	0.215	0.404	0.212	0.018	0.144	0.891	0.548	0.427	0.957	0.357	0.687
		3	0.600	0.000	0.201	0.364	0.190	0.112	0.133	0.766	0.497	0.391	0.817	0.217	0.582
	2	1	0.600	0.000	0.209	0.411	0.189	0.041	0.149	0.952	0.560	0.399	0.932	0.332	0.644
		2	0.600	0.000	0.185	0.383	0.228	0.045	0.159	1.037	0.542	0.413	0.924	0.324	0.610
		3	0.600	0.010	0.219	0.426	0.183	0.040	0.122	0.885	0.548	0.403	0.917	0.317	0.648
		4	0.600	0.000	0.193	0.387	0.214	0.055	0.151	0.870	0.538	0.407	0.907	0.307	0.642
		5	0.600	0.001	0.207	0.409	0.208	0.025	0.151	1.186	0.560	0.415	0.957	0.357	0.600
		6	0.600	0.016	0.222	0.386	0.208	0.028	0.140	0.812	0.526	0.430	0.924	0.324	0.676
		7	0.600	0.000	0.216	0.413	0.205	0.022	0.144	0.988	0.557	0.421	0.962	0.362	0.663
		8	0.600	0.000	0.187	0.349	0.230	0.070	0.165	0.969	0.513	0.417	0.881	0.281	0.587
		9	0.600	0.001	0.220	0.396	0.198	0.074	0.111	0.718	0.507	0.418	0.871	0.271	0.650
		10	0.600	0.001	0.207	0.404	0.214	0.037	0.136	0.909	0.541	0.421	0.934	0.334	0.658
6–2	2	1	0.500	0.010	0.165	0.286	0.305	0.056	0.178	2.923	0.464	0.470	0.876	0.376	0.017
		2	0.500	0.001	0.122	0.297	0.188	0.249	0.143	1.951	0.440	0.310	0.638	0.138	0.060
		3	0.500	0.073	0.170	0.385	0.178	0.088	0.107	1.925	0.492	0.348	0.754	0.254	0.184
		4	0.500	0.061	0.119	0.305	0.205	0.111	0.199	1.626	0.504	0.324	0.746	0.246	0.262
		6	0.500	0.048	0.217	0.353	0.209	0.096	0.076	1.168	0.430	0.426	0.748	0.248	0.398
		7	0.500	0.002	0.186	0.422	0.188	0.112	0.090	2.596	0.513	0.374	0.818	0.318	0.054
		8	0.500	0.000	0.189	0.353	0.253	0.096	0.110	1.499	0.462	0.442	0.829	0.329	0.382
		10	0.500	0.053	0.132	0.264	0.227	0.178	0.146	1.774	0.410	0.359	0.641	0.141	0.114
7	2	2	0.400	0.000	0.229	0.491	0.167	0.000	0.112	1.370	0.604	0.396	1.000	0.600	0.590
		4	0.400	0.062	0.194	0.309	0.274	0.083	0.078	0.825	0.387	0.468	0.728	0.328	0.476
		5	0.400	0.013	0.176	0.490	0.175	0.001	0.145	1.405	0.635	0.351	0.978	0.578	0.559
	3	2	0.400	0.039	0.184	0.307	0.281	0.134	0.055	2.203	0.362	0.465	0.677	0.277	0.027
		3	0.400	0.110	0.148	0.287	0.237	0.075	0.143	0.866	0.430	0.385	0.699	0.299	0.435

Table 3 Continued

Sample #	Runs	Spot	X_{NaCl}	a_1	a_2	a_3	a_4	a_5	a_6	r	a_{Na}	a_{NaCa}	$a_{Na}/(1-a_{NaCa})$	X_{NaCl}	Calculated X_{NaCl}
		4	0.400	0.002	0.147	0.253	0.348	0.117	0.133	1.260	0.385	0.495	0.763	0.363	0.385
		7	0.400	0.020	0.198	0.241	0.357	0.079	0.106	1.340	0.347	0.555	0.779	0.379	0.378
		8	0.400	0.012	0.199	0.368	0.240	0.030	0.150	1.334	0.519	0.439	0.925	0.525	0.525
		9	0.400	0.004	0.210	0.331	0.257	0.000	0.197	1.279	0.528	0.467	0.992	0.592	0.608
		11	0.400	0.015	0.224	0.402	0.193	0.000	0.166	1.169	0.568	0.417	0.974	0.574	0.622
		12	0.400	0.003	0.212	0.487	0.203	0.037	0.057	2.144	0.545	0.415	0.931	0.531	0.297
8	7	4	0.300	0.023	0.164	0.270	0.292	0.143	0.108	1.302	0.378	0.456	0.695	0.395	0.305
	8	1	0.300	0.027	0.266	0.409	0.166	0.080	0.053	1.157	0.461	0.432	0.812	0.512	0.464
		4	0.300	0.000	0.238	0.444	0.185	0.072	0.062	1.610	0.506	0.422	0.876	0.576	0.397
	10	1	0.300	0.000	0.165	0.321	0.256	0.000	0.258	1.758	0.579	0.421	1.000	0.700	0.478
		6	0.300	0.067	0.138	0.230	0.264	0.000	0.300	2.306	0.530	0.403	0.888	0.588	0.207
		14	0.300	0.035	0.179	0.313	0.237	0.074	0.163	1.295	0.477	0.415	0.815	0.515	0.427
		20	0.300	0.000	0.172	0.383	0.259	0.000	0.185	1.258	0.568	0.432	1.000	0.700	0.623
	11	1	0.300	0.110	0.180	0.306	0.246	0.000	0.157	1.070	0.464	0.426	0.808	0.508	0.485
9-2	1	3	0.200	0.038	0.214	0.436	0.204	0.049	0.059	2.942	0.494	0.418	0.849	0.649	−0.015
	6	2	0.200	0.000	0.199	0.394	0.262	0.034	0.111	1.547	0.505	0.462	0.938	0.738	0.477
		4	0.200	0.034	0.210	0.469	0.132	0.131	0.025	1.156	0.494	0.342	0.750	0.550	0.402
		5	0.200	0.003	0.226	0.458	0.100	0.167	0.046	1.408	0.504	0.326	0.748	0.548	0.327
		6	0.200	0.008	0.223	0.421	0.135	0.106	0.108	2.263	0.528	0.358	0.823	0.623	0.155
		7	0.200	0.000	0.234	0.479	0.151	0.000	0.137	2.178	0.616	0.384	1.000	0.800	0.357
11-3	1	1	0.000	0.067	0.378	0.000	0.473	0.081	0.000	0.027	0.000	0.851	0.000	0.000	−0.020
		3	0.000	0.075	0.396	0.000	0.471	0.058	0.000	0.037	0.000	0.867	0.000	0.000	−0.024
		4	0.000	0.030	0.389	0.000	0.581	0.000	0.000	0.000	0.000	0.970	0.000	0.000	−0.013

* See text for meaning of the parameters.

$$X_{NaCl} = a_{Na}/(1-a_{NaCa}) - (0.294\,r + 0.014) \quad (5)$$

Plotting the X_{NaCl} values calculated from equation (5) (for $r \leq 1$) against the actual X_{NaCl} values of individual samples shows a well-defined liner correlation (Fig. 9), with the interception close to zero (0.007±0.023) and the slope close to 1 (0.993±0.030). It is therefore suggested that equation (5) can be used to estimate X_{NaCl} from Raman spectra of partly frozen fluid inclusions, as long as the degree of freezing is above certain level (i.e., $r \leq 1$).

5 Discussion

In the study of geologic processes involving fluids, it is important to know the composition of the geologic fluids. The compositional system of the geologic fluids may be estimated from the eutectic temperature of the fluid inclusions representing the paleo-fluids (e.g., Crawford, 1981). However, it has been shown that the eutectic temperatures are difficult to determine, because the first melting temperature may be related to various meta-stability phenomena and recrystallization process, and does not necessarily reflect eutectic melting (Davis et al., 1990). Therefore, it is generally not reliable to use the first melting temperatures to estimate the compositional system of fluid inclusions. The cryogenic Raman spectroscopic analysis provides an excellent tool for determining the fluid compositional system, as different salt hydrates can be distinguished by their Raman bands (Dubessy et al., 1982, 1992; Samson and Walker, 2000; Bakker, 2004; Derome et al., 2005; Baumgartner and Bakker, 2009a and b; 2010). However, it is generally not satisfactory to just know the compositional system; it is important to know the proportions of different salts in the solutions. Although this may be achieved by measuring the melting temperatures of different hydrates with microthermometry, it has been shown to be a time consuming and often futile method due to the difficulty to visually distinguish different solid phases in the fine hydrates-ice aggregates. It would be ideal if we could correlate the intensities of the Raman peaks of different salt-hydrates with the proportions of salts in the solution, so that the major solute composition of fluid inclusions can be estimated by cryogenic Raman spectroscopy. Such a work has been attempted in a previous study (Samson and Walker, 2000), but no quantitative results have been achieved mainly because of the difficulty to completely freeze the fluid

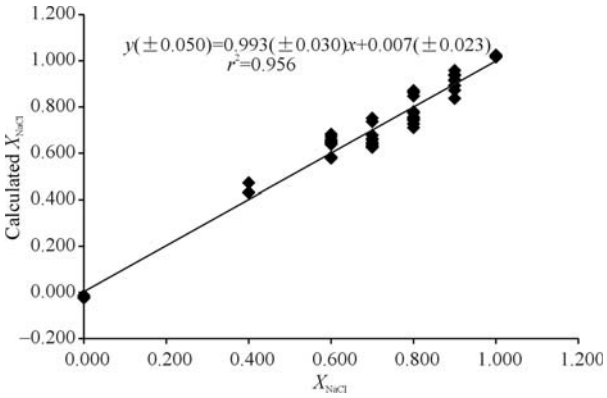

Fig. 9. Correlation between the actual X_{NaCl} of the solution (prepared) and X_{NaCl} calculated from equation (5).

inclusions. In this study, we were able to achieve complete freezing by adding alumina powder to the solutions, and established a linear correlation between the X_{NaCl} values of H_2O-NaCl-$CaCl_2$ solutions and the fraction of peak areas of hydrohalite among all the hydrates. This linear correlation is consistent with theoretical prediction based on the assumption of a homogeneous, isotropic (i.e., random orientation of crystals) hydrates-ice aggregate, and indicates that cryogenic Raman spectroscopy can be used to study the proportions of monoatomic ions (Na^+, Ca^{2+}, and Mg^{2+}) in geologic fluids, as long as the fluids can be completely frozen. The spread of the analysis results (Table 1 and Fig. 3), which is reflected by the standard deviation of the calculated X_{NaCl} (Fig. 3b), is most likely due to local inhomogeneity and anisotropy related to the crystal sizes of the hydrates. This problem may be resolved by using scanning Raman spectroscopy in the future.

6 Conclusions

Although complete freezing can be realized by adding alumina powder into the solution in the sandwiched experiments, incomplete freezing is common for synthetic (silica capillary) and natural fluid inclusions, as previously recognized (Samson and Walker, 2000). Our experiments further confirm that even if a fluid inclusion looks like completely frozen, as shown by increased darkness and the grainy texture, it may contain only ice crystals and interstitial solution and no hydrates. In this case, the composition of the fluid inclusion (X_{NaCl}) cannot be estimated with Raman analysis at all. If some hydrates were precipitated but a large amount of solution remained, as indicated by the elevated "water bump" in the Raman spectra, X_{NaCl} cannot be estimated with Raman analysis either; in other words, the fraction of hydrohalite peaks among all the hydrates is not proportional to the X_{NaCl} in the original solution. However, if the amount of remaining solution is limited, as indicated by a relatively small "water bump" (i.e., the area of the "water bump" is less than the total area of all hydrate peaks), the fractionation of NaCl between the solid phases and the remaining solution may be "corrected" to give a linear relationship between the fraction of hydrohalite peaks and X_{NaCl}. The uncertainties in X_{NaCl} estimation using this method, as reflected by the spread of the calculated X_{NaCl} values and the standard deviation (Fig. 9), are most likely related to local inhomogeneity of the solid-solution mixture as well as the peak area calculation procedure (Fig. 6). This method provides a new tool to estimate the salt composition of fluid inclusions, has the advantage of non-destructive single inclusion analysis, and can be used to complement microthermometry. However, it should be pointed out that this method cannot be directly applied to fluid inclusions containing halite daughter mineral, because the hydrates formed from freezing are not proportional to the bulk fluid compositions. It is also worth noting that the potential errors in estimating X_{NaCl} values are fairly large, as indicated in Figures 8 and 9.

In conclusion, the cryogenic Raman spectroscopic studies of H_2O-NaCl-$CaCl_2$ solutions reveals a linear correlation between X_{NaCl} and the intensities of Raman bands attributed to hydrohalite, confirming the theoretical expectation that the fraction of NaCl molecules in the solution (i.e., X_{NaCl}) is equal to the fraction of NaCl•$2H_2O$ molecules in the aggregates of salt hydrates if the solution is completely frozen. The results further indicate that even if the solution is not completely frozen, as is common for fluid inclusions, X_{NaCl} can still be estimated from the Raman spectra, as long as the incompleteness of freezing is below certain level. This provides a new, non-destructive method to estimate the salt composition for single fluid inclusions.

Acknowledgements

This study was supported by an NSERC-Discovery grant (to Chi), and in part by the Knowledge Innovation Program of Chinese Academy of Sciences (SIDSSE-201302). The use of trade, product, industry, or firm names in this report is for descriptive purpose only and does not constitute endorsement by the University of Regina and the Chinese Academy of Sciences. Constructive reviews by three anonymous reviewers have improved the paper.

Manuscript received Mar. 14, 2014
accepted June 13, 2014
edited by Hao Qingqing

References

Azmy, K., Lavoie, D., Knight, I., and Chi, G., 2008. Dolomitization of the Aguathuna Formation Carbonates of Port au Port Peninsula in Western Newfoundland, Canada: Implications for a Hydrocarbon Reservoir. *Canadian Journal of Earth Sciences*, 45: 795–813.

Bakker, R.J., 2004. Raman spectra of fluid and crystal mixtures in the system H_2O, H_2O–NaCl and H_2O–$MgCl_2$ at low temperatures: applications to fluid inclusion research. *Canadian Mineralogist*, 42: 1283–1314.

Banks, D.A., and Yardley, B.W.D., 1992. Crush-leach analysis of fluid inclusions in small natural and synthetic samples. *Geochimica et Cosmochimica Acta*, 56: 245–248.

Baumgartner, M., and Bakker, R.J., 2009a. Raman spectroscopy of pure H_2O and NaCl–H_2O containing synthetic fluid inclusions in quartz - a study of polarization effects.

Mineralogy and Petrology, 95: 1–15.

Baumgartner, M., and Bakker, R.J., 2009b. $CaCl_2$-hydrate nucleation in synthetic fluid inclusions. *Chemical Geology*, 265: 335–344.

Baumgartner, M., and Bakker, R.J., 2010. Raman spectra of ice and salt hydrates in synthetic fluid inclusions. *Chemical Geology*, 275: 58–66.

Chi, G., and Ni P., 2007. Equations for calculation of NaCl/($NaCl+CaCl_2$) ratios and salinities from hydrohalite-melting and ice-melting temperatures in the H_2O-NaCl-$CaCl_2$ system. *Acta Petrologica Sinica*, 23: 33–37.

Chi, G., and Savard, M.M., 1995. Fluid evolution and mixing in the Gays River carbonate- hosted Zn-Pb deposit and its surrounding barren areas, Nova Scotia. *Atlantic Geology*, 31: 141–152.

Chi, G., and Savard, M.M., 1997. Sources of basinal and Mississippi Valley-type mineralizing brines: Mixing of evaporated seawater and halite-dissolution brine. *Chemical Geology*, 143: 121–125.

Chi, G., Guha, J., and Lu, H.-Z., 1993. Separation mechanism in the formation of proximal and distal tin-polymetallic deposits, Xinlu ore field, southern China - Evidence from fluid inclusion data. *Economic Geology*, 88: 916–933.

Chi, G.X., Chou, I.-M., and Lu, H.Z., 2003a. An overview on current fluid-inclusion research and applications. *Acta Petrologica Sinica*, 19: 201–212.

Chi, G., Giles, P.S., Williamson, M.A., Lavoie, D., and Bertrand, R., 2003b. Diagenesis and porosity evolution of Upper Carboniferous sandstones from the Spring Valley #1 Well, Maritimes Basin, Canada – implications for reservoir development. *Journal of Geochemical Exploration*, 80/2-3: 171–191.

Chi, G., Kontak, D.J., and Williams-Jones, A.E., 1998. Fluid composition and thermal regime during base-metal mineralization in the lower Windsor Group, Nova Scotia. *Economic Geology*, 93: 883–895.

Chi, G., Savard, M.M., and Héroux, Y., 1995. Constraints from fluid inclusion data on the origin of the Jubilee carbonate-hosted Zn-Pb deposit, Cape Breton, Nova Scotia. *Canadian Mineralogist*, 33: 709–721.

Chou, I.M., Song, Y., and Burruss, R.C., 2008. A new method for synthesizing fluid inclusions in fused silica capillary containing organic and inorganic material. *Geochimica et Cosmochimica Acta*, 72: 5217–5231.

Crawford, M.L, 1981. Phase equilibria in aqueous fluid inclusions. In: Holister, L.S., and Crawford, M.L. (eds.), *Fluid Inclusions: Applications to Petrology*. *Mineralogical Association of Canada Short Course Handbook*, 6: 75–100.

Davis, D.W., Lowenstein, T.K., and Spencer R.J., 1990. Melting behavior of fluid inclusions in laboratory-grown halite crystals in the systems NaCl-H_2O, NaCl-KCl-H_2O, NaCl-$MgCl_2$-H_2O, and NaCl-$CaCl_2$-H_2O. *Geochimica et Cosmochimica Acta*, 54 : 591–601.

Derome, D., Cathelineau, M., Cuney, M., Fabre, C., and Lhomme, T., 2005. Mixing of sodic and calcic brines and uranium deposition at McArthur River, Saskatchewan, Canada: A Raman and laser-induced breakdown spectroscopic study of fluid inclusions. *Economic Geology*, 100: 1529–1545.

Dubessy, J., Audeoud, D., Wilkins, R., and Kosztolanyi, C., 1982. The use of the Raman microprobe Mole in the determination of the electrolytes dissolved in the aqueous phase of fluid inclusions. *Chemical Geology*, 37: 137–150.

Dubessy, J., Poty, B., and Ramboz, C., 1989. Advances in C–O–H–N–S fluid geochemistry based on micro-Raman spectrometric analysis of fluid inclusions. *European Journal of Mineralogy*, 1: 517–534.

Dubessy, J., Boiron, M.C., Moissette, A., Monnin, C., and Stretenskaya, N., 1992. Determination of water, hydrates and pH in fluid inclusions by micro-Raman spectrometry. *European Journal of Mineralogy*, 4: 885–894.

Dubessy, J., L'Homme, T., Boiron, M.C., and Rull F., 2002. Determination of chlorinity in aqueous fluids using Raman spectroscopy of the stretching band of water at room temperature: application to fluid inclusions. *Applied Spectroscopy*, 56: 99–106.

Fabre, C., Boiron, M. C., Dubessy, J., and Moissette, A., 1999. Determination of ions in individual fluid inclusions by laser ablation optical emission spectroscopy: development and applications to natural fluid inclusions. *Journal of Analytical Atomic Spectrometry*, 14: 913–922.

Frezzotti, M.L., Tecce, F., and Casagli, A., 2012. Raman spectroscopy for fluid inclusion analysis. *Journal of Geochemical Exploration*, 112: 1–20.

Gleeson, S.A., Wilkinson, J. J., Stuart, F. M., and Banks, D.A., 2001. The origin and evolution of base metal mineralizing brines and hydrothermal fluids, South Cornwall, UK. *Geochimica et Cosmochimica Acta*, 65: 2067–2079.

Gunther, D., Audetat, A., Frischknecht, R., and Heinrich, C.A., 1998. Quantitative analysis of major, minor and trace elements in fluid inclusions using laser ablation – inductively coupled plasma mass spectrometry. *Journal of Analytical Atomic Spectrometry*, 13: 263–270.

Haynes, F.M., 1985. Determination of fluid inclusion composition by sequential freezing. *Economic Geology*, 80: 1436–1439.

Haynes, F.M., and Kesler, S.E., 1987. Chemical evolution of brines during Mississippi valley type mineralization: evidence from East Tennessee and Pine Point. *Economic Geology*, 82: 53–71.

Kontak, D.J., 2004. Analysis of evaporate mounds as a complement to fluid-inclusion thermometric data: case studies from granitic environments in Nova Scotia and Peru. *Canadian Mineralogist*, 42: 1315–1329.

Lavoie, D., and Chi, G., 2010. Lower Paleozoic foreland basins in eastern Canada: tectono-thermal events recorded by faults, fluids and hydrothermal dolomites. *Bulletin of Canadian Petroleum Geology*, 58: 17–35.

Lavoie, D., and Chi, G., Brennan-Alpert, P., Desrochers, A., Bertrand, R., 2005. Hydrothermal dolomitization in the Lower Ordovician Romaine Formation of the Anticosti Basin: Significance for hydrocarbon exploration. *Bulletin of Canadian Petroleum Geology*, 53: 454–471.

Lai, J.Q, Chi, G.X., Peng, S.L, Shao, Y.J., and Yang, B., 2007. Fluid evolution in the formation of the Fenghuangshan Cu-Fe-Au deposit, Tongling, Anhui, China. *Economic Geology*, 102: 949–970.

Leisen, M., Dubessy, J., Boiron, M.-C., and Lach, P., 2012. Improvement of the determination of element concentrations in fluid inclusion by LA-ICP-MS based on the Pitzer's thermodynamic equation and error calculations. *Geochimica et Cosmochimica Acta*, 90: 110–125.

Li, H., Xi, X.S., Wu, C.M., and Watanabe, K., 2013. Genesis of

the Zhaokalong Fe-Cu polymetallic deposit at Yushu, China: Evidence from ore geochemistry and fluid inclusions. *Acta Geologica Sinica*, 87: 486–500.

Lu, W.J., Chou, I.-M., Burruss, R.C., and Song, Y.C., 2007. A unified equation for calculating methane vapor pressures in the CH4–H_2O system with measured Raman shifts. *Geochimica et Cosmochimica Acta*, 71: 3969–3978.

Mernagh, T.P., and Wilde, A.R., 1989. The use of the laser Raman microprobe for the determination of salinity in fluid inclusions. *Geochimica et Cosmochimica Acta*, 53: 765–771.

Ni, P., Ding, J., and Rao, B., 2006. In situ cryogenic Raman spectroscopic studies on the synthetic fluid inclusions in the systems H_2O and NaCl–H_2O. *Chinese Science Bulletin*, 51: 108–114.

Oakes, C.S., Bodnar, R.J., and Simonson, J.M., 1990. The system NaCl–$CaCl_2$–H_2O: 1. The ice liquidus at 1 atm total pressure. *Geochimica et Cosmochimica Acta*, 54: 603–610.

Rosso, K. M., and Bodnar, R. J., 1995. Microthermometric and Raman spectroscopic detection limits of CO2 in fluid inclusions and the Raman spectroscopic characterization of CO_2. Geochimica et Cosmochimica Acta, 59: 3961–3975.

Pasteris, J.D., Wopenka, B., and Seitz, J.C., 1988. Practical aspects of quantitative laser Raman microprobe spectroscopy for the study of fluid inclusions. *Geochimica et Cosmochimica Acta*, 52: 979–988.

Samson, I.M., and Walker, R.T., 2000. Cryogenic Raman spectroscopic studies in the system NaCl–$CaCl_2$–H_2O and implications for low-temperature phase behavior in aqueous fluid inclusions. *Canadian Mineralogist*, 38: 35–43.

Samson, I.M., Williams-Jones, A.E., Ault, K.M., Gagnon, J.E., and Fryer, B.J., 2008. Source of fluids forming distal Zn–Pb–Ag skarns: evidence from laser ablation-inductively coupled plasma-mass spectrometry analysis of fluid inclusions from El Mochito, Honduras. *Geology*, 36: 947–950.

Savard, M.M., and Chi, G., 1998. Cation study of fluid inclusion decrepitates in the Jubilee and Gays River Zn-Pb deposits - Characterization of ore-forming brines. *Economic Geology*, 93: 920–931.

Song, Y., Chou, I.M., Hu, W., Burruss, R.C., and Lu, W., 2009. CO_2 density-Raman shift relation derived from synthetic inclusions in fused silica capillaries and its application. *Acta Geologica Sinica*, 83: 932–938.

Steele-MacInnis, M., Bodnar, R.J., and Naden, J., 2011. Numerical model to determine the composition of H_2O–NaCl–$CaCl_2$ fluid inclusions based on microthermometric and microanalytical data. *Geochimica et Cosmochimica Acta*, 75: 21–40.

Sun, Q., Zhao, L., Li, N., and Liu, J., 2010. Raman spectroscopic study for the determination of Cl-concentration (molarity scale) in aqueous solutions: application to fluid inclusions. *Chemical Geology*, 272: 55–61.

Vanko, D.A., Bodnar, R.J., and Sterner, S.M., 1988. Synthetic fluid inclusions: VIII. Vapor-saturated halite solubility in part of the system NaCl–$CaCl_2$–H_2O, with application to fluid inclusions from oceanic hydrothermal systems. *Geochimica et Cosmochimica Acta*, 52: 2451–2456.

Wang, X.L., Chou, I.-M., Hu, W.X., Burruss, R.C., Sun, Q., and Song, Y., 2011. Raman spectroscopic measurements of CO_2 density: Experimental calibration with high-pressure optical cell (HPOC) and fused silica capillary capsule (FSCC) with application to fluid inclusion observations. *Geochimica et Cosmochimica Acta*, 75: 4080–4093.

Wang, X.L., Hu, W.X., and Chou, I.-M., 2013. Raman spectroscopic characterization on the OH stretching bands in NaCl–Na_2CO_3–Na_2SO_4–CO_2–H_2O systems: Implications for the measurement of chloride concentrations in fluid inclusions. Journal of Geochemical Exploration, 132: 111–119.

Wendte, J., Al-Aasm, I., Chi, G., and Sargent, D., 2009. Fault/fracture controlled hydrothermal dolomitization and associated diagenesis of the Upper Devonian Jean Marie Member (Redknife Formation) in the July Lake area of northeastern British Columbia. *Bulletin of Canadian Petroleum Geology*, 57: 275–322.

Williams-Jones, A.E., and Samson, I.M., 1990. Theoretical estimation of halite solubility in the system NaCl–$CaCl_2$–H_2O: applications to fluid inclusions. *Canadian Mineralogist*, 28: 299–304.

Xue, C.J., Zeng, R., Liu, S.W., Chi, G.X., Qing, H.R., Chen, Y.C., Yang, J.M., and Wang, D.H., 2007. Geologic, fluid inclusion and isotopic characteristics of the Jinding Zn-Pb deposit, western Yunnan, South China: A review. *Ore Geology Review*, 31: 337–359.

Xue, W., Xue, C.J., Chi, G.X., Shi, H.G., Gao, B.Y., and Yang, S.F., 2010. A study of fluid inclusions from the Baiyangping polymetallic deposit in the Lanping basin, northwestern Yunnan, China. *Acta Petrologica Sinica*, 26: 1173–1184 (in Chinese with English abstract).

Yang, Y.P., Zheng, H.F., and Zhang, L.F., 2009. Determining pressure with daughter minerals in fluid inclusion by Raman spectroscopy: sphalerite as an example. *Acta Geologica Sinica*, 83: 628–632.

Zheng, H.F., Qiao, E.W., Yang, Y.P., and Duan, T.Y., 2011. Determination of inner pressure for fluid inclusions by Raman spectroscopy and its application. *Geoscience Frontiers*, 2: 403–407.

About the first author

Guoxiang Chi was born in 1963 in Longyan, Fujian Province, China. He received his B.Sc. from Fuzhou University in 1983, M.Sc. from Changsha Institute of Geotectonics, Chinese Academy of Sciences in 1986, and Ph.D. from University of Quebec in Chicoutimi, Canada in 1992. His research interest is mainly in the field of fluid geochemistry and hydrodynamics in relation to metallic mineralization and hydrocarbon accumulation, with emphasis on application of fluid-inclusion, stable isotope, and numerical modeling techniques.

E-mail at guoxiang.chi@uregina.ca.